Macromolecules **1995**, *28*, 6029–6041

Structures of Oxyethylene/Oxybutylene Diblock Copolymers in Their Solid and Liquid States

Yung-Wei Yang, Siriporn Tanodekaew, Shao-Min Mai, and Colin Booth

Department of Chemistry, University of Manchester, Manchester M13 9PL, U.K.

Anthony J. Ryan*

Manchester Materials Science Centre, UMIST, Grosvenor Street, Manchester M1 7HS, U.K., and CLRC Daresbury Laboratory, Warrington WA4 4AD, U.K.

Wim Bras[†]

NWO and CLRC Daresbury Laboratory, Warrington WA4 4AD, U.K.

Kyriakos Viras

Physical Chemistry Laboratory, Department of Chemistry, National and Kapodistrian University of Athens, Panepistimiopolis, 157 71 Athens, Greece

Received February 24, 1995; Revised Manuscript Received June 7, 1995[®]

ABSTRACT: A series of ethylene oxide/1,2-butylene oxide diblock copolymers (E_mB_n) was synthesized. Across the series, the oxyethylene E-block length was approximately constant (m = 26–32 units) and the oxybutylene B-block length varied (B_n, n = 3–30 units). All copolymers had narrow chain length distributions ($M_w/M_n < 1.08$). The melts were investigated by small-angle X-ray scattering (SAXS), and the semicrystalline solids were investigated by SAXS, wide-angle X-ray scattering (WAXS), and low-frequency Raman spectroscopy. The melting behavior of the solids was investigated by differential scanning calorimetry (DSC). The SAXS patterns found for the liquid copolymers were consistent with disordered systems, with the melts of the longer copolymers close enough to the order–disorder transition to show substantial contributions from composition fluctuations in a system of unstretched chains. In the solid state, copolymers with $n \le 20$ formed lamellae in which the whole chain was in extended conformation, i.e. the E blocks crystallized in their usual helical conformation, and extended B blocks formed a liquid-crystalline array. For a copolymer with a longer B block (n = 30), the E blocks crystallized in once-folded conformation, while the B blocks remained extended.

1. Introduction

Block copolymers are of fundamental scientific interest and also find use as highly-functional, added-value products in a wide range of industrial and biomedical applications, such as surfactants and gelling agents in aqueous systems, compatibilizers in polymer blends, viscosity modifiers in lubricating oils, and food additives.[1–5] The unique properties of polyurethane foam rely on it being formed from a block copolymer.[1,6] The field was initiated by the introduction of the Pluronic range of copolymers of ethylene oxide and propylene oxide by Wyandotte Chemical Co. in 1951[7] and was further stimulated by the announcement of the first thermoplastic elastomers, block copolymers of styrene and isoprene, by Shell Chemical Co. in 1961.[8]

The useful properties of block copolymers originate largely from the tendency of blocks to segregate, giving rise to diverse structures, which range from micelles in dilute solution, through various lyotropic liquid-crystalline states based on packed micelles, to the microphase-separated structures which are characteristic of block copolymers in their bulk (i.e. solid and melt) states.[5] Consequently, there is much interest in investigating the effect across a wide range of materials and conditions, and particularly in the application of the recently developed technique of simultaneous small-angle and wide-angle X-ray scattering (SAXS/WAXS) coupled with differential scanning calorimetry (DSC).

In this report we consider the structures of diblock copolymers of ethylene oxide and 1,2-butylene oxide in the bulk state. The copolymers are denoted E_mB_n, where E represents an oxyethylene unit [OCH_2CH_2] and B an oxybutylene unit [$OCH_2CH(CH_2CH_3)$]. A limited range of related copolymers are presently marketed by the Dow Chemical Co.,[9] but those used in the present work were synthesized in our laboratory. Consideration has already been given[10] to the structures formed from these copolymers in the micellar and gel states of their aqueous solutions. In the bulk state, the oxyethylene block is crystallizable and the oxybutylene block, which is atactic in microstructure,[11] is noncrystallizable. The melting points of the copolymers lie in the range 40–50 °C, and both the solid (semicrystalline) and liquid (noncrystalline) microphases of the copolymers are conveniently accessible to experiment.

1.1. Liquid Copolymers. The microphase-separation behavior of noncrystallizable (liquid) block copolymers was first documented many years ago.[12] In the ordered melt, diblocks form periodic structures with length scale $d = 2\pi/q^*$, giving rise to a peak at q^* in the X-ray scattering pattern. Here $q = (4\pi/\lambda)\sin(\theta/2)$, where λ is the wavelength of the radiation and θ is the scattering angle.

Theoretical and experimental aspects of microphase separation have been recently reviewed.[5,13] Starting from the pioneering studies of Helfand and Wasserman[14] and Liebler,[15] major contributions have come from self-consistent mean-field theories. Considering an AB block copolymer comprising $N = N_A + N_B$ chain units, each occupying the same volume (v) and having

---

[†] Current address: AMOLF, Kruislaan 407, 1098 SJ Amsterdam, The Netherlands.

[®] Abstract published in *Advance ACS Abstracts,* July 15, 1995.

0024-9297/95/2228-6029$09.00/0

the same statistical length (b), theory predicts equilibrium microphase behavior dependent only on the product χN (where χ is the Flory–Huggins parameter) and the composition defined by the mole fraction of (e.g.) A chain units, $x_A = N_A/N$. For this special case, parameter b is uniquely determined by the radius of gyration of the copolymer,

$$R_g^2 = Nb^2/6 \qquad (1)$$

and parameter χ by the noncombinatorial Gibbs energy of mixing

$$\Delta_{mix}G_{nc} = kT(\chi N)x_A x_B \qquad (2)$$

For the copolymers of interest here, the unlike segments mix endothermically, and the temperature dependence of χ will be given approximately by

$$\chi = \alpha T^{-1} + \beta \qquad (3)$$

where α and β are positive constants dependent on composition. Phase separation is favored by lowering the temperature.

The main features of microphase separation in such a block copolymer system are clear. At low values of χN the block copolymer comprises a single disordered phase in which the chains have unperturbed dimensions.[13,15] Connectivity leads to a characteristic correlation length scaling as the radius of gyration, i.e. as $N^{0.5}$. Microphase separation is predicted at $\chi N \approx 10$. The boundary is known either as the microphase-separation transition (MST) or as the order–disorder transition (ODT). The condition $\chi N \approx 10$ defines the weak segregation limit, WSL, of the ordered system. As the ODT is approached, theory[16] predicts fluctuations in the disordered phase, for which experiment has shown[17] characteristic dimensions scaling in the range $N^{0.5}$ to $N^{0.8}$. Immediately beyond the boundary (i.e. in the WSL), limited demixing of A and B occurs to form a microphase-separated system with characteristic dimension variously predicted[17–20] to scale as $N^{0.8}$ to $N^{0.95}$. Far from the ODT, in the strong segregation limit (SSL, $\chi N \gg 10$), AB contacts are limited to a narrow interfacial region, the microphases are essentially pure A and pure B, and the characteristic length is invariably predicted[13] to scale as $N^{0.67}$.

In the SSL, any decrease in Gibbs energy resulting from minimization of interfacial area must be balanced against the resulting increase in Gibbs energy from the more extended chain conformation. Hence, at equilibrium in the SSL, the major phase-separated structures of bcc spheres, hexagonally-packed cylinders, and lamellae depend only on composition.[12] In the WSL, theory[15] accounts for the same structures, but the complex mesophases (phases intermediate between the predicted structures) recently observed in weakly segregated diblocks[21–23] are not predicted.

The assumption of equal volume and equal statistical length are overly restrictive in the application of theory to many block copolymers, including the E_mB_n copolymers of present interest. The problem has been discussed in a number of recent papers.[21,24,25] In the Flory–Huggins treatment of mixtures of two polymers, eq 2 is recast in terms of volume fraction (ϕ) and the number of segments (r_v). The two types of segments (E and B) each have the same reference volume, v_0. For systems comprising E and B units, it is convenient to use the volume occupied by an E unit (v_E) as reference, whence

$$r_v = r_{vE} + r_{vB} = N_E + N_B(v_B/v_E) \qquad (4)$$

where v_B is the volume occupied by a B unit. Room temperature values of the densities of liquid poly(oxyethylene) and poly(oxybutylene)[26,27] lead to a value of $v_B/v_E \approx 1.89$. With values of χ based on the same reference volume, the equation for the noncombinatorial part of the free energy of mixing per chain, analogous to eq 2, is

$$\Delta_{mix}G_{nc} = kT(\chi r_v)\phi_E\phi_B \qquad (5)$$

where ϕ_E and ϕ_B are volume fractions. This formulation requires a phase diagram plotted as χr_v versus, e.g., ϕ_E. If the two types of segment defined by volume have equal statistical lengths, and if parameter χ is independent of concentration, then this phase diagram will be symmetrical in ϕ_E.

Asymmetry in the phase diagram is caused by a difference in statistical lengths, which enters through the radius of gyration. Corresponding to eq 4, the unperturbed square radius of gyration is referenced to r_s segments of identical statistical length (b_o), in the present case put equal to that of an E unit: i.e.

$$R_g^2 = r_s b_E^2/6 \qquad (6)$$

where

$$r_s = r_{sE} + r_{sB} = N_E + N_B(b_B^2/b_E^2) \qquad (7)$$

With the chain length expressed in segments defined by volume,

$$R_g^2 = [r_{vE} + r_{vB}(v_E b_B^2/v_B b_E^2)](b_E^2/6) = [r_{vE} + \epsilon r_{vB}](b_E^2/6) \qquad (8)$$

where parameter $\epsilon = (v_E b_B^2/v_B b_E^2)$ is equivalent to that described by Vavasour and Whitmore[20,25] and similar to that described by Amdahl *et al.*[21] Reported[28,29] values of the unperturbed dimensions of poly(oxyethylene) and poly(oxybutylene) lead to $b_B^2/b_E^2 \approx 1.22$, whence $\epsilon \approx 0.65$. This is close to the value (i.e. $\epsilon = 0.6$) used by Vavasour and Whitmore[25] to illustrate the changes in the phase diagram to be expected from limited copolymer asymmetry, e.g. that typical of poly(styrene)–poly(diene) block copolymers. Following that work, it would be predicted that the microphase-separation (disorder–order) boundary in the present system would be little changed from the hypothetical symmetrical case, but that the order–order boundaries would be affected, being significantly shifted toward higher volume fractions of oxyethylene (E): compare Figure 1 of ref 25 with that of ref 20.

1.2. Solid Copolymers. For low-molar-mass copolymers, it may be taken for granted that crystallization of one block will result in separation into lamellar microphases, as the negative free energy of crystallization will greatly outweigh the free energy of dislocation of any microphase-separated structure in the melt. Copolymers with one glass-forming block are exceptions to this rule, since a structure formed in the melt in the temperature interval between the glass transition temperature of one block and the crystallization temperature of the other may persist in a metastable solid state: e.g. diblock copolymers of ethylene oxide and styrene[30,31] or ethylene and styrene.[32] Both components of the present E_mB_n copolymers have low glass transition temperatures ($T_g < -60$ °C) , and the crystalline structure should be independent of any structure in the melt. Recent experiments on mobile systems with microphase-separated melts, e.g. butadiene/ϵ-caprolactone copolymers,[33] have shown that this is generally the case. Cylindrical morphologies have been reported[34] for crystalline poly(dimethylsiloxane)/poly(oxyethylene) copolymers with lengthy E blocks. Any possibility of crystal morphology being influenced by liquid morphology can be avoided by studying block copolymers with homogeneous melts, e.g. ethylene and ethylene-*alt*-propylene.[35,36]

Some understanding of the possible equilibrium morphologies of crystallizable block copolymers comes from studies of uniform oligomers with two crystallizable components. In oligo(oxyethylene)−oligo(methylene) systems, it has been shown that initial crystallization of the oxyethylene block in helical conformation (area of cross-section per chain = 21.4 Å^2) allows subsequent crystallization of trans-planar alkyl blocks, whereas initial crystallization of trans-planar alkyl blocks (area of cross-section per chain = 18.4 Å^2) precludes crystallization of the oxyethylene block: see refs 37 and 38 and references therein. The layer crystals formed had their oligomeric blocks locally crystalline or liquid-crystalline as appropriate, and also locally normal or tilted relative to the layer end-group plane. Related structures were found for low-molar-mass nonuniform ($M_n < 3000$ g mol^{-1}, $M_w/M_n < 1.10$) oxyethylene−methylene block copolymers,[39] but in that case the initial crystallization of one component essentially precluded crystallization of the other, this being a direct result of disorder at the block interface. This effect in nonuniform block copolymers with two crystallizable components was first recorded many years ago by Perret and Skoulios in their pioneering studies of diblock copolymers of ethylene oxide and ϵ-caprolactone,[40] and has been remarked upon many times since, e.g. ref 5.

The importance of specific factors in determining chain packing in the crystalline and noncrystalline microphases of block copolymers warns against a general theory. This is certainly the case when dealing with low-molar-mass copolymers, particularly when the crystallizable blocks are incorporated into the lamellae in unfolded-chain conformation. The ongoing flux of noncrystallizable chains of the second block has to be accommodated, and the ratio of areas of cross-section of the two types of block is an important consideration if space is to be filled at normal densities. Published theories[41−43] recognize this competition between preferred low-free-energy conformations, i.e. unfolded chains for the crystallized component and randomly-coiled chains for the noncrystallized component, and minimize the Gibbs energy by introducing an equilibrium degree of chain folding in the crystalline layer. In particular, Whitmore and Noolandi have made detailed calculations for the solid-state structures of diblock copolymers of styrene and ethylene oxide.[42]

A study by differential scanning calorimetry of the fusion of $E_mB_nE_m$ triblock copolymers has been reported recently.[44] We are not aware of any investigation of the structures of E_mB_n diblock copolymers. Solid-state structures of low-molar-mass oxyethylene/oxypropylene block copolymers, and associated thermodynamic properties of fusion, have been reported for both diblock (E_mP_n)[45] and triblock ($P_nE_mP_n$)[46−49] copolymers. Like oxybutylene blocks, oxypropylene blocks formed by anionic polymerization are atactic.[50] A combination of SAXS and low-frequency Raman spectroscopy (i.e. determination of LAM-1 frequency) was used[48] to show that $P_nE_mP_n$ copolymers with short E blocks (i.e. m = 39 or 48) and n in the range 1−10 crystallized with their E blocks in unfolded-chain conformation, but with the chains (or parts of the chains) significantly tilted with respect to the lamellar end plane for copolymers with lengthy P blocks. Chain folding was important only for $P_nE_mP_n$ block copolymers with longer E blocks: e.g. 75 units.

Block lengths and purities of E_nP_n copolymers prepared by anionic polymerization of propylene oxide are limited by a transfer reaction.[51] Accordingly, copolymers of ethylene oxide and butylene oxide were used in the present study, as the anionic polymerization of butylene oxide takes place without transfer,[10,11] which makes possible the preparation of pure copolymers with lengthy B blocks.

The diblock copolymers (E_mB_n) used in the present work had $m \approx 30$ and n in the range 3−31. As described below, this range of compositions gave access to phase-separated structures in the solid state ($T < T_m$) and interesting effects in the liquid state ($T > T_m$). In choosing this copolymer series, we were conscious of the possibility of fractionation by chain length during crystallization of a distribution of short chains, and also of chain folding in the crystallization of long chains (referred to above). The number-average lengths of the present copolymers in chain atoms (C and O) ranged from 99 ($E_{30}B_3$) to 183 ($E_{31}B_{30}$). Studies of uniform chains has allowed precise determination of the critical length for chain folding. Uniform n-alkanes crystallize from the melt in the once-folded-chain conformation when somewhat longer than 168 chain atoms.[52,53] Uniform oligo(oxyethylene) dialkyl ethers behave similarly: e.g. $C_{15}E_{45}C_{15}$ (166 chain atoms) crystallizes with unfolded chains, while $C_{18}E_{45}C_{18}$ (172 chain atoms) crystallizes with once-folded chains.[54] The choice of a series of copolymers based on E_{30} represented a compromise between fractionation and chain-folding effects. As will be demonstrated below, the strategy was reasonably effective.

The present study was based primarily on the simultaneous WAXS/SAXS/DSC technique for investigation of copolymer structures in their melt and solid states. However, a complete study required additional information. Accordingly, the question of chain folding in the crystalline state was addressed by considering the SAXS results in combination with LAM-1 frequencies from low-frequency Raman spectroscopy, while additional precision was brought to the thermal analysis by means of conventional DSC.

2. Experimental Section

2.1. Preparation and Characterization of Copolymers. The copolymers were prepared by sequential anionic polymerization, first of ethylene oxide and then of 1,2-butylene oxide. The methods of preparation and characterization have been described in detail previously.[10,55] Vacuum line and ampule techniques were used throughout in order to minimize initiation by moisture of unwanted difunctional chains.

The poly(oxyethylene) precursors (sampled after completion of the first stage of polymerization) and the final copolymers were all characterized by gel permeation chromatography (GPC) and ^{13}C NMR spectroscopy. NMR assignments were taken from previous work.[11] The GPC curves, which contained single narrow peaks, were analyzed to provide values of the

Table 1. Molecular Characteristics of E_mB_n Block Copolymers[a]

copolymer	M_{pk}/g mol^{-1} (GPC)	M_w/M_n (GPC)	M_n/g mol^{-1} (NMR)	x_E/mol % (NMR)	w_E (NMR)
$E_{32}B_3$	1530	1.04	1620	0.91	0.87
$E_{27}B_6$	1770	1.05	1630	0.82	0.73
$E_{30}B_7$	1680	1.03	1820	0.81	0.72
$E_{28}B_9$	1930	1.08	1920	0.76	0.66
$E_{32}B_{10}$	2150	1.03	2130	0.76	0.66
$E_{29}B_{11}$	1950	1.05	2070	0.69	0.62
$E_{26}B_{13}$	2140	1.08	2080	0.67	0.55
$E_{27}B_{17}$	2500	1.06	2410	0.61	0.49
$E_{29}B_{20}$	2750	1.08	2710	0.59	0.47
$E_{31}B_{30}$	3310	1.06	3520	0.51	0.39

[a] M_{pk} = molar mass corresponding to the peak of the GPC curve; M_w/M_n = ratio of weight- to number-average molar mass from GPC; M_n = number-average molar mass from NMR. Estimated uncertainties: M_{pk} to ±10%; M_w/M_n to ±0.03; M_n and mol % E to ±3%.

molar mass corresponding to the elution volume at the peak [M_{pk}, calibration with poly(oxyethylene) standards] and the ratio of weight-average to number-average molar mass, M_w/M_n, a measure of the width of the chain length distribution. Correction was made for instrumental spreading. ^{13}C NMR spectroscopy provided accurate values of M_n by end-group analysis, as well as copolymer compositions.

The ^{13}C NMR spectra were also used to ensure purity of the samples. The purities of the precursor copolymers were verified by comparing the intensities of resonances from hydroxy-end-group carbons with those from initiator carbons: in all cases these intensities were identical within experimental error. Similarly, the purities of the block copolymers were checked by comparing the intensities of resonances from end-group carbons with those from carbons associated with EB block junctions. In some samples a small excess (<3%) of hydroxy end groups over EB junctions was found. This was attributed to formation of homopoly(oxybutylene) initiated by a small amount of moisture introduced with the second charge of monomer. These copolymers were purified, either by reprecipitating them from solution in dichloromethane at room temperature by adding hexane or by repeatedly equilibrating them with warm hexane and separating the solid and liquid phases after cooling to 10 °C. Homopoly(oxybutylene) was efficiently removed by either procedure. All samples were dried under vacuum (<0.01 mmHg, 25 °C, >12 h) and stored under refrigeration at 10 °C.

Molecular characteristics of the copolymers used are given in Table 1. The formulas were calculated from the values of M_n of the poly(oxyethylene) blocks determined by NMR after stage one of the synthesis and the overall compositions of the copolymers determined by NMR after purification. We estimate uncertainties of ±1 in the block lengths.

2.2. Simultaneous SAXS/WAXS/DSC. Measurements were made on beamline 8.2 of the SRS at the SERC Daresbury Laboratory, Warrington, U.K. Details of the storage ring, radiation and camera geometry and data collection electronics have been given elsewhere.[56] The camera was equipped with a multiwire quadrant detector (SAXS) located 3.5 m from the sample position and a curved knife-edge detector (WAXS) that covered 120° of arc at a radius of 0.3 m. A vacuum chamber placed between the sample and detectors reduced air scattering and absorption. Both the exit window of the beam line and the entrance window of the vacuum chamber were made from 15 μm mica, and the exit windows of the vacuum chamber were made from 15 μm mica and 50 μm Kapton film for the WAXS and SAXS detectors, respectively. The WAXS detector had a spatial resolution of 50 μm and could handle up to ~100 000 counts s^{-1}; only 90° of arc was active in the present experiments, the rest of the detector being shielded with lead. The spatial resolution of the SAXS detector was 400 μm and it could handle up to ~500 000 counts s^{-1}. A beam stop was mounted just before the exit window to prevent the direct beam from hitting the SAXS detector, which measured intensity in the radial direction (over an opening angle of 70° and an active length of 0.2 m) and was only suitable for isomorphous scatterers.

The specimens for SAXS/WAXS/DSC were placed in a TA Instruments DSC pan containing a 0.75 mm brass spacer ring and fitted with windows (ca. 7 mm diameter) made from 25 μm thick mica. The loaded pans were placed in the cell of a Linkam DSC of single-pan design. The cell comprised a silver furnace around a heat-flux plate with a 3 × 0.5 mm slot, the sample being held in contact with the plate by a low-thermal-mass spring. A reference (calibration) sample pan of the same thermal mass was first subjected to the temperature ramp and the thermal response of this neutral system was recorded. The thermal response of the sample pan was then recorded, and the differential response was calculated. The single pan technique relies on the accuracy and reproducibility of the temperature control system. The present system was comparable in precision to a conventional, two-pan, heat-flux DSC (e.g. a DuPont 990). A more complete description of the DSC and the sample pans can be found elsewhere.[57,58] In the present experiments, the temperature program was as follows: heat from 5 to 50–60 °C at either 5 or 10 K min^{-1}, hold at 50–60 °C for 1 min, and cool at the same rate as the heating cycle to 5 °C.

The scattering pattern from an oriented specimen of wet collagen (rat-tail tendon) was used to calibrate the SAXS detector, and high-density polyethylene, aluminum, and an NBS silicon standard were used to calibrate the WAXS detector. Parallel plate ionization detectors placed before and after the sample cell recorded the incident and transmitted intensity. The experimental data were corrected for background scattering (subtraction of the scattering from the camera, hot stage, and an empty cell), sample thickness, and transmission, and for any departure from positional linearity of the detectors.

The data acquisition systems for SAXS/WAXS and DSC comprised separate computers. The PC-based controller for the DSC initiated the SAXS/WAXS data collection once the first control temperature was reached. The beam-line data acquisition system had a time-frame generator which collected the SAXS/WAXS data in 6 s frames separated by a wait time of 10 μs. During the wait time a high-voltage pulse was written over the DSC signal in order to have exact time correlation between the SAXS/WAXS and DSC data.[58]

2.2.1. Data Analysis. In all analyses it was assumed that the samples, whether melts or polycrystalline solids, had small domains relative to the sample size and, therefore, were isotropic with respect to the X-ray pattern: i.e. all orientations were adequately sampled in the one-dimensional experiments.

SAXS: Liquid State. The scattering patterns from samples in the liquid state were analyzed by plotting $I(q)$ vs q and taking the centroid of the peak as q^*. Where possible, the assignment of q^* was confirmed by fitting the peaks with a Gaussian function.

SAXS: Solid State. A Lorentz correction, q^2, was applied to the observed SAXS intensity to obtain a Lorentz-corrected intensity Iq^2. Subtraction of the background, as described previously,[59] gave corrected intensity $I'q^2$. Lamellar spacings (Bragg spacings) were calculated from the position (q^*) of the first-order maximum in $I'q^2$ versus q, so that $d_c = (2\pi/q^*)$.

SAXS Invariant. The invariant Q, i.e. the total intensity of SAXS from the system, was calculated throughout each experiment. Determination of the absolute invariant (Q) required absolute intensity measurements, thermal background subtraction, and extrapolation to $q = 0$ and ∞ and was computationally difficult to achieve. Accordingly, a relative invariant (Q', arbitrary units) was calculated as the area under the $I'q^2$ versus q curve between the first reliable data point, $q = 0.007$ Å^{-1}, and the region in which $I'q^2$ became constant ($q \geq 0.20$ Å^{-1} in the present experiments), i.e.

$$Q' = \int_{0.007}^{0.020} I'(q)\, q^2\, \mathrm{d}q \qquad (9)$$

It has been shown[59] that the major contributions to Q are adequately reflected in Q'.

WAXS: Solid State. Peaks in the WAXS patterns were indexed to the crystal structure of poly(oxyethylene).[60] An internal comparison method, comparing the integrated intensities associated with crystalline and amorphous features, was used to calculate a degree of crystallinity. The assumption that the total scattering within a region of reciprocal space was independent of the state of aggregation of the polymer allowed approximate calculation of a degree of crystallinity (mass fraction) from

$$X_W = A_C/A \qquad (10)$$

where A_C is the area assigned to the sharp peaks originating from crystalline polymer and A is the total area under the scattering pattern, including the contribution from the underlying amorphous halo, A_L. A Simpson rule integration was used because peak shapes were partly instrument limited, and any fitting routine had to be a convolute of both the instrument resolution and the scattering intensity. The integrated intensity over the main peaks gave a value of A_C and the integrated intensity over an adjacent range without peaks gave a value of A_L, hence an estimate of A. Without performing numerical analysis over the whole pattern, and in the absence of any method of external calibration, the method gave only semiquantitative information, i.e. an estimated uncertainty of 20%.

2.3. Raman Spectroscopy. Raman scattering at 90° to the incident beam was recorded by means of a Spex Ramalog spectrometer fitted with a 1403 double monochromator, and with a third (1442U) monochromator operated in scanning mode. The light source was a Coherent Innova 90 argon-ion laser operated at 514.5 nm and 500 mW. Typical operating conditions for the low-frequency range under investigation were: bandwidth 1.5 cm^{-1}, scanning increment 0.05 cm^{-1}, integration time 4 s. The low-frequency scale was calibrated to ±0.1 cm^{-1} by reference to the 9.4 and 14.9 cm^{-1} bands in the spectrum of L-cystine. High-frequency spectra were also recorded for each sample.

Crystalline samples were held in the hollowed end of a stainless-steel rod, in which they were melted and cooled rapidly to room temperature to crystallize. Spectra were recorded with the samples at room temperature, i.e. approximately 20 °C. Precise control of temperature was not sought, as the temperature derivative of frequency is known[61] to be small for the LAM-1 bands of poly(oxyethylene).

2.4. Differential Scanning Calorimetry. A Perkin-Elmer DSC-4 was used. Dry samples of the copolymers (ca. 10 mg) were taken from storage at 10 °C and sealed under drybox conditions at room temperature into aluminum pans. These samples were cooled in the calorimeter to 0 °C and heated at 10 K min^{-1} to ~60 °C. The molten samples were then cooled to 0 °C at a controlled rate, in the range −1 to −10 K min^{-1}, before reheating to 60 °C. Replicate experiments were performed with heating rates in the range +1 to +10 K min^{-1}. Certain samples were self-seeded by heating to 40 °C for a period up to 1 h before quenching to 0 °C.

Melting temperatures were obtained as the temperatures at the peaks of endotherms, and enthalpies of fusion were obtained from peak areas. The temperature and power scales of the calorimeters were calibrated by melting indium, and the temperature calibration was checked by melting point standards. Melting temperatures obtained using different heating rates were in substantial agreement provided that correction was made for thermal lag, for example, a lag of ca. 2 K at 10 K min^{-1}. Enthalpies of fusion were independent of heating rate.

3. Results and Discussion

3.1. General Features of the WAXS/SAXS/DSC Experiments. Copolymers $E_{30}B_7$, $E_{32}B_{10}$, $E_{26}B_{13}$, $E_{27}B_{17}$, $E_{29}B_{20}$, and $E_{31}B_{30}$ were investigated by simultaneous WAXS/SAXS/DSC. General features of the measurements are illustrated in Figures 1 to 3. Three-dimensional relief diagrams of time-resolved SAXS and WAXS from copolymer $E_{27}B_{17}$ are shown in Figures 1 and 2. Similar results, showing related patterns of melting and rapid recrystallization, were obtained for the other samples investigated. Crystallization, whether observed by SAXS/WAXS/DSC or by conventional DSC, was rapid under all conditions employed. Crystallization rates were not further investigated.

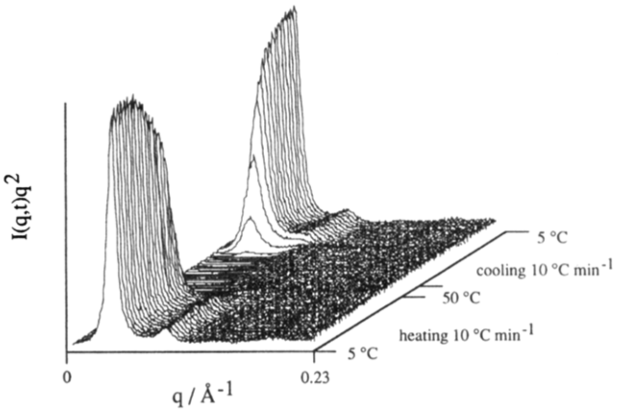

Figure 1. Three-dimensional relief diagram of time-resolved SAXS data obtained with a time resolution of 6 s during melting and recrystallization of copolymer $E_{27}B_{17}$. The heating cycle was 5 °C → 50 °C → 5 °C at a ramp rate of 10 K min^{-1}. The plot shows Lorentz-corrected SAXS intensity, $I(q,t)q^2$, versus scattering vector, q, versus temperature, T.

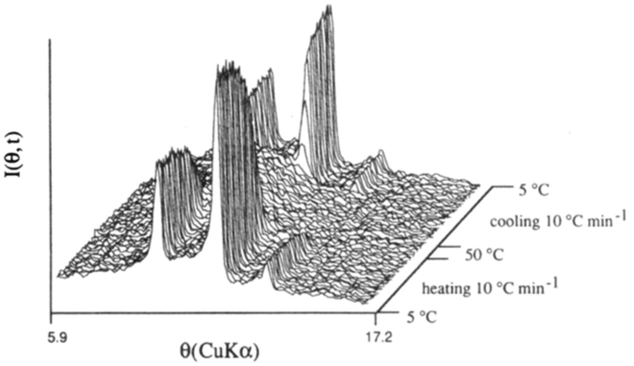

Figure 2. Three-dimensional relief diagram of time-resolved WAXS data obtained with a time resolution of 6 s during melting and recrystallization of copolymer $E_{27}B_{17}$. The heating cycle was 0 °C → 50 °C → 0 °C at a ramp rate of 10 K min^{-1}. The plot shows WAXS intensity, $I(2\theta,t)$, versus scattering vector, q, versus temperature, T.

The peaks in the WAXS scattering patterns indexed satisfactorily to the crystal structure of poly(oxyethylene), i.e. to the monoclinic subcell of the structure with alternating right-hand and left-hand 7/2 helices.[60] This crystal structure was also confirmed by high-frequency Raman spectroscopy using the assignments of Matsuura and Fukuhara.[62]

SAXS results for the all the crystalline samples showed scattering patterns characteristic of lamellar stacks. For example, 4 orders of reflection with equal spacing were seen in the scattering curves of crystalline copolymer $E_{27}B_{17}$: see Figure 1. The scattering patterns from the melt were more difficult to interpret. Broad peaks were observed in the region $0.05 \leq q \leq 0.15$ Å^{-1} of the SAXS patterns for all copolymers except $E_{30}B_7$. This point is made more clearly in Figure 3, in which SAXS patterns found for both crystalline and molten samples of copolymers $E_{30}B_7$ and $E_{26}B_{13}$ are contrasted. Possible interpretations are considered in the next section.

3.2. Structures of the Liquid Copolymers. SAXS patterns of melts of the six copolymers at 50 °C are

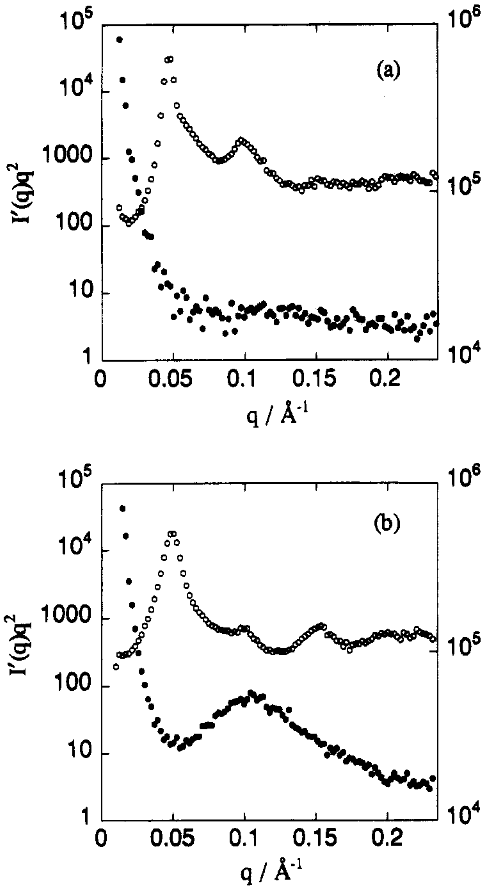

Figure 3. Lorentz-corrected SAXS patterns of crystalline copolymer ($I(q)q^2$ versus q, left-hand axis, sample at 10 °C) and uncorrected SAXS patterns for molten copolymer ($I(q)$ versus q, right-hand axis, sample at 50 °C). The semilogarithmic plots are for copolymers (a) $E_{30}B_7$ and (b) $E_{26}B_{13}$. The results for the crystalline copolymers show clearly either 2 or 4 orders of reflection from lamella stacks. The plot for molten copolymer $E_{26}B_{13}$ shows a broad scattering peak, whereas that for copolymer $E_{30}B_7$ shows no scattering peak.

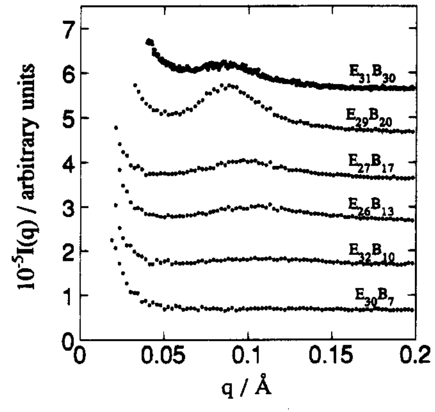

Figure 4. SAXS patterns ($I(q)$ versus q) for the molten copolymers (T = 50 °C). The $I(q)$ scale is arbitrary. For clarity, results are displaced on the ordinate by 10^5.

illustrated in Figure 4. The scattering curves for copolymers $E_{30}B_7$ to $E_{29}B_{20}$ were obtained on the same day under identical conditions, and the arbitrary intensity scales are directly comparable. That for copolymer $E_{31}B_{30}$ was measured on a separate occasion. The length scales (d_l) obtained from five curves with detectable scattering peaks are listed in Table 2.

The most likely interpretation of the results described above is that all the liquid copolymers were disordered but that the melts of the longer copolymers were close enough to the ODT to show substantial contributions to SAXS from composition fluctuations,[16,17] whereas those of the shorter copolymers ($E_{32}B_{10}$ and, particularly, $E_{30}B_7$) were further from the order–disorder transition and showed a much weaker fluctuation effect. Because of the low molar mass of the copolymers used in this study, very little scattering would be expected from correlation in an otherwise homogeneous melt.[15]

Table 2. SAXS from E_mB_n Block Copolymer Melts:[a] T = 50 °C

copolymer	d_l/Å	ϕ_E	r_v	r_s
$E_{30}B_7$		0.694	43.2	38.5
$E_{32}B_{10}$	58	0.629	50.9	44.2
$E_{26}B_{13}$	59	0.511	50.6	41.9
$E_{27}B_{17}$	63	0.456	59.1	47.7
$E_{29}B_{20}$	71	0.434	66.8	53.4
$E_{31}B_{30}$	74	0.353	87.7	67.6

[a] d_l = Bragg spacing from SAXS: uncertainty, ±3 Å. ϕ_E = volume fraction of E in liquid copolymer = $w_E/[(w_E + w_B(\varrho_E/\varrho_B)]$, $\varrho_E/\varrho_B = 1.155$. $r_v = m + 1.889n$ = segment length of copolymer based on the volume of an E unit: uncertainty, ±3. $r_s = m + 1.22n$ = segment length of copolymer based on the statistical length of an E unit: uncertainty, ±3.

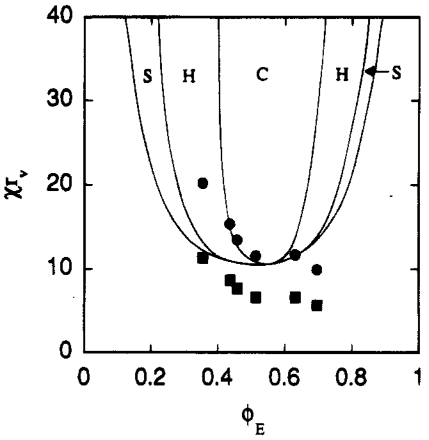

Figure 5. Microphase transition diagram from ref 20 for a liquid block copolymer system with asymmetry parameter ϵ = 0.6. Data points for copolymers $E_{30}B_7$ to $E_{31}B_{30}$ are calculated for (●) $\chi = 0.23$ and (■) $\chi = 0.13$, as indicated in the text.

It is unlikely that the peaks originate from microphase separation. However, uncertainty arises through not knowing values of the interaction parameter χ. As discussed in the Introduction, the microphase transition diagram expected for the liquid EB system can be taken to be that calculated by Vavasour and Whitmore[25] for a block copolymer with asymmetry parameter $\epsilon = 0.6$: see Figure 5. In order to place the present copolymers on the diagram, it is necessary to know values of χ for the EB system. The required values have not been reported, but the related poly(oxyethylene)–poly(oxypropylene) system has been investigated.[63–65] In that system, χ at $T \approx 30$ °C was found[65] to be approximately 0.1 and to vary slightly with concentration: i.e.

$$\chi = 0.10 - 0.02\phi_E \qquad (11)$$

where values are referred to a segment volume equal to that of an E unit. The slight concentration dependence arises mainly from the difference in shape of the two units, the segment–segment interaction being surface fraction dependent rather than volume fraction dependent.[64] Adjustment of the temperature to 50 °C would reduce this value by about 5%.

It can be assumed that values of χ for the EB system are larger than those found for the EP system. We consider just two possibilities.

(A) All the copolymer melts are disordered. This requires a value of $\chi < 0.14$, as illustrated by the filled squares in Figure 5, which were positioned assuming that $\chi = 0.13$.

(B) The four copolymer melts giving rise to prominent scattering peaks are ordered; i.e. the ODT lies between copolymers $E_{32}B_{10}$ and $E_{26}B_{13}$. This requires the value of $\chi > 0.2$, as illustrated by the filled circles in Figure 5, which were positioned assuming that $\chi = 0.23$. The prediction is that the ordered liquid copolymers separate into either lamellar or E cylinders.

There are several reasons for preferring case A over case B. A value of χ for the EB system not more than 50% larger than that of the EP system seems more likely than the higher value needed for microphase separation. Additionally, there are a number of features of the SAXS from the melts (see Figure 4) which argue against microphase separation. (i) The SAXS data extend out to $q = 0.23$ Å^{-1} and yet there is no obvious indication of higher order reflections: e.g. a second-order reflection would be expected for $E_{27}B_{20}$ at $q = 0.18$ Å^{-1}. (ii) The peaks are broad, with $\Delta q/q^* \approx 0.5$ (where Δq is the full width half-maximum), whereas well-ordered materials typically[36] have $\Delta q/q^* \ll 0.1$. (iii) The peak shapes are Gaussian, whereas Lorentzian peaks would be expected for well-ordered materials.[36] Points i–iii may be less important for the present low-molar-mass copolymers than for the high-molar-mass copolymers usually studied, since there may be a greater contribution to peak broadening from chain length distribution.

The different compositions and chain lengths of the copolymers place them at different distances below the microphase-separation boundary in the diagram (see Figure 5). It is known that there is a region of fluctuations below the microphase-separation transition. According to Frederickson and Helfand's[16] correction to Liebler's theory,[15] its size in the phase diagram scales as $N^{-1/3}$, making it most important for short chains. If we characterize the copolymers in terms of their distances below the ODT, i.e. by a parameter δ defined as

$$\delta = 1 - \chi N/\chi N_{\mathrm{ODT}}$$

then that with the highest value of δ (i.e. copolymer $E_{30}B_7$) will be unlikely to have large amplitude density fluctuations and, hence, should not show a prominent peak in its SAXS pattern. The gradual change in the SAXS patterns, seen in Figure 4, provides evidence of a gradual change rather than a sharp boundary between "fluctuation" and "correlation" behavior, in agreement with small-angle neutron scattering results for polyolefins.[17]

The validity of our interpretation was explored further by considering the relationship of the characteristic dimenions ($d_l = 2\pi/q^*$) of fluctuations in the melts to the statistical segment lengths (r_s) of the copolymers. The appropriate log–log plot is shown in Figure 6a. The best line through the points has a slope of 0.54 ± 0.12. The considerable uncertainty arises from the scatter in just five points, not least the difficulty in locating the peak for copolymer $E_{32}B_{10}$. Scaling as $r_s^{0.5}$ is consistent with fluctuations in a melt of unstretched chains.[16,17]

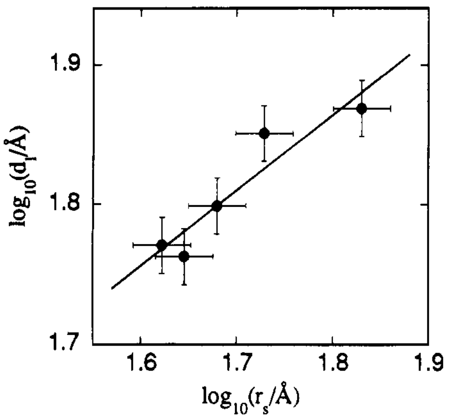

Figure 6. Logarithm of periodicity SAXS spacing ($\log_{10} d_l$) plotted against the logarithm of statistical segment length ($\log_{10} r_s$) for molten block copolymers $E_{26}B_{13}$ to $E_{31}B_{30}$ ($T = 50$ °C). The straight line (slope 0.54 ± 0.12) was calculated by least squares.

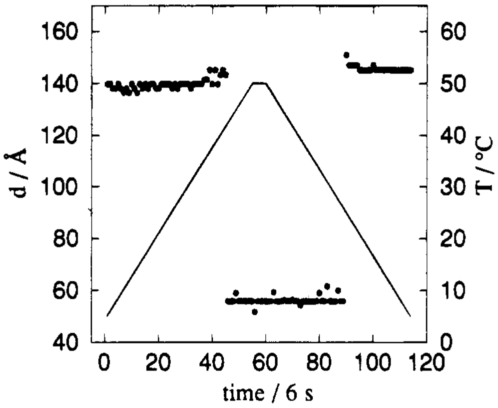

Figure 7. Spacing versus experiment time from SAXS recorded every 6 s through the heating and cooling cycle: i.e. 10 K min^{-1} from 5 to 50 °C, hold for 1 min at 50 °C, cool at 10 K min^{-1} from 50 to 5 °C. Note that the lamellar spacing of the crystalline copolymer is essentially constant over a given temperature region but that the initial lamellar spacing is not exactly regenerated on cooling.

The analogous plot for ordered systems requires that account be taken of Bragg scattering for hexagonally packed cylinders of copolymer $E_{31}B_{30}$, since the periodicity in that case is $(2/\sqrt{3})d_l$. The relevant log–log plot (not shown) has a best line though the points of 0.84 ± 0.10, i.e. in acceptable agreement with theoretical predictions for ordered copolymer melts near the WSL. However, the balance of the evidence greatly favors the melts of the copolymers being close to the ODT but disordered.

In the above discussion we have considered values of χ only in relation to the "mean-field" microphase transition diagram shown in Figure 5, which does not take account of fluctuations. For copolymers of the type considered here, the fluctuation theory of Fredrickson and Helfand[16] predicts that the transition could occur at $\chi r_v \approx 20$ ($\phi_E = 0.5$), rather than at $\chi r_v \approx 10$, which could double the value of χ required for microphase separation. This consideration further confirms our conclusion that the copolymers melted directly into the disordered phase.

3.3. Microphase Separation in the Solid Copolymers. 3.3.1. Lamellar Spacings from SAXS. The reversible nature of the semicrystalline to liquid transition can be seen in Figure 7, where the lamella spacing of sample $E_{27}B_{17}$ calculated from the peak position as $d_c = 2\pi/q^*$ is plotted against time over its heating and cooling cycle. The circles are the lamella spacings (left-hand axis) and the line is the nominal temperature profile (right-hand axis). The first-order transitions from a spacing characteristic of extended-chain lamellar

Table 3. Crystalline E_mB_n Block Copolymers: WAXS, SAXS, and Raman Scattering[a]

copolymer	d_c/Å	l_c/nm	ν_1/cm^{-1}
$E_{32}B_3$		104	9.7
$E_{27}B_6$		100	9.7
$E_{30}B_7$	130, 120	113	9.1
$E_{28}B_9$		114	8.2
$E_{32}B_{10}$	161, 157	129	7.7
$E_{29}B_{11}$		124	7.7
$E_{26}B_{13}$	127, 145	123	
$E_{27}B_{17}$	138, 147	140	7.0
$E_{29}B_{20}$	166, 166	157	6.5
$E_{31}B_{30}$	152, 153	199	7.8

[a] d_c = Bragg spacing from SAXS: uncertainty, ±1.5 Å. First value for sample as received, second value for sample after recrystallization. l_c = calculated extended chain length = $0.97z_E + 1.21z_B$ (see text): uncertainty, ±4 Å. ν_1 = LAM-1 frequency from Raman spectroscopy: uncertainty, ±0.5 cm^{-1}.

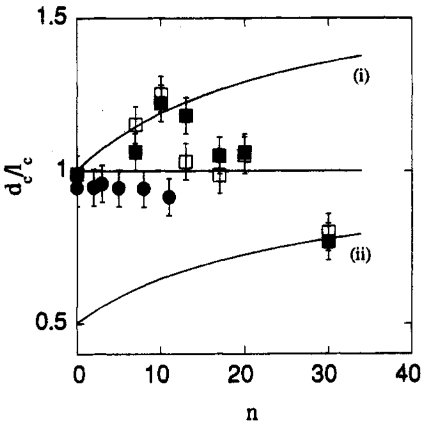

Figure 8. Ratio of lamellar spacing (d_c) to calculated molecular length (l_c) for as-received (□) and recrystallized (■) E_mB_n and (●) E_mP_n block copolymers plotted against B- or P-block length (n) as appropriate. The lamellar spacings were obtained by SAXS. The molecular lengths were calculated for a fully-extended chain with a helical E block and a trans-planar B block. The curves correspond to lamellae of type i or ii, as described in the text.

crystals (extended molecular length $l_c \approx 140$ Å) to one characteristic of a microphase-separated liquid is obvious in the data. Because of the difference in thermal history, recrystallization gave a spacing slightly different from that found for the initial material. As discussed more fully in section 3.3.3, there is the possibility of fractionation during crystallization of these copolymers. Within ±2 Å, replicate heating and cooling runs gave the same value of d_c, i.e. that characteristic of the recrystallized sample.

Lamellar spacings obtained for the six copolymers investigated by SAXS (d_c) are listed in Table 3. Values are given for both initial and recrystallized samples. Comparison is made with approximate molecular lengths (l_c) calculated for isolated extended chains with E blocks in helical conformation and B blocks in trans-planar conformation, the formula used being

$$l_c \approx 0.97z_E + 1.21z_B \qquad (12)$$

where z_E and z_B are numbers of chain atoms (C and O), 0.97 Å is the length per chain atom along the oxyethylene helix axis,[66] and 1.21 Å is length per chain atom along the trans-planar axis (an average value for C−C and C−O bonds).[67] Both sets of values (from Table 3) were used to calculate the ratios d_c/l_c which are plotted against B-block length (n) in Figure 8.

The area of cross-section of the crystalline poly(oxyethylene) helix is approximately 21 Å^2, while that of poly(oxybutylene) in an ordered array of trans-planar extended chains at normal liquid density at 20 °C ($v_B \approx$ 74 cm^3 mol^{-1}) is

$$(10^{24}v_B)/(3.63N_A) \approx 34\ \text{Å}^2 \qquad (13)$$

This disparity in cross-sectional area must be taken into account in considering packing E_mB_n block copolymers in extended chain conformation into lamallae. Considering a simple model of a lamella (crystalline and noncrystalline layers), crystallization of the E blocks in a uniform array, such that $d_c = l_c$, could take place only at the expense of a high density in the B layer. We envisage alleviation of this packing problem either (i) by disruption of a uniform array of fully-extended chains so as to maintain normal density or (ii) by folding of the E block. Accordingly, comparison was made between the experimental results and those expected for simple models corresponding to states i and ii identified above.

(i) Lamellae composed of fully-extended chains which are oriented normal to the lamellar end plane but which are irregularly packed so as to maintain normal crystalline-E and liquid-B densities. Calculated lamellar spacing (Å) = $0.97z_E/\phi_E$, where ϕ_E = volume fraction of E in the semicrystalline copolymer.

(ii) Lamellae composed of regularly-packed chains with B-blocks extended and E-blocks once folded, which are oriented normal to the lamellar end plane. Calculated lamellar spacing (Å) = $0.485z_E + 1.21z_B$.

Spacings calculated in this way are plotted relative to the fully-extended chain length in Figure 8. Comparison of calculated and experimental ratios indicates that model i applies at short B-block lengths (≤B_{13}), and model ii at long B-block lengths (B_{30}). Copolymers with intermediate block lengths show transitional behavior, probably as a result of forming lamellae containing both extended and folded E blocks. Mixed stacks of lamellae with exclusively extended or folded E blocks is another possibility. The lamellar spacings obtained confirm that the extended E-block conformation dominates in the range B_{13}−B_{20} and are consistent with chain folding of the E block in copolymer $E_{30}B_{30}$. Unequivocal evidence of this chain folding is presented in section 3.3.2.

A corresponding calculation for oxypropylene chains ($v_P \approx$ 58 cm^3 mol^{-1}) leads to an area of cross-section of the extended trans-planar chain of 26 Å^2. An investigation of $E_{40}P_n$ copolymers ($n \leq 11$)[45] showed that the relatively small disparity in chain-unit volume could be accommodated without undue disruption of the ordered lamellae, and with only a small increase in density in the "liquid" layer, i.e. much as expected for parallel packing of chains in a liquid-crystalline layer. The different behaviors of the two systems can be seen from the SAXS results shown in Figure 8: within experimental error the lamella spacings for the E_mP_n copolymers with P-block length as high as P_8 are very nearly those expected for uniformly-packed fully-extended chains.

3.3.2. Chain Conformation from Raman Spectroscopy. High-frequency Raman spectra were consistent with the E-blocks being crystallized in their usual helical conformation, the indicators used[62] being the bands at 291, 936, and 1231 cm^{-1}. These high-frequency spectra were taken before and after recording the low-frequency spectra, thus confirming the stability of the samples in the laser beam.

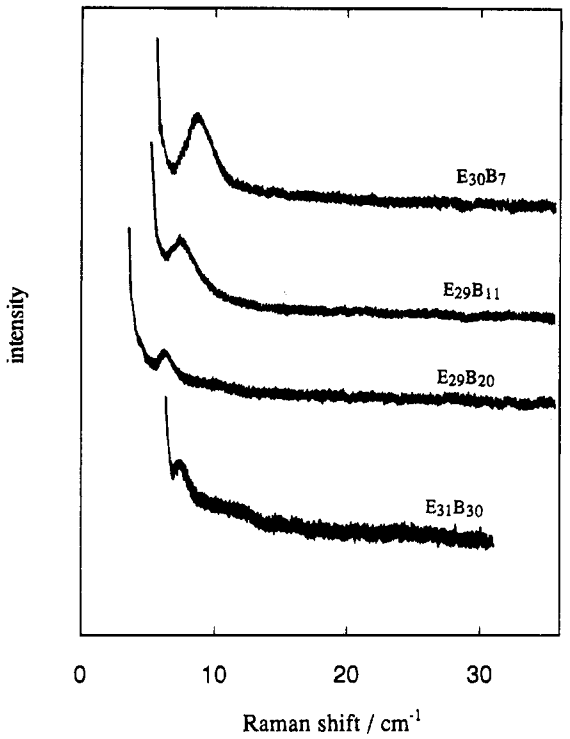

Figure 9. Low-frequency Raman spectra of crystalline copolymers $E_{30}B_7$, $E_{29}B_{11}$, $E_{29}B_{20}$, and $E_{31}B_{30}$ (as indicated). The intensity scales and zeros are arbitrary.

Combination of SAXS with low-frequency Raman spectroscopy allowed unambiguous assignment of chain conformation in the crystalline copolymers. The frequency of the single-node longitudinal vibrational mode (acoustic mode, LAM-1) was determined. Assuming uniform extended chains with free ends, the LAM-1 frequency (ν_1) should be related inversely to chain length through

$$\nu_1/\mathrm{cm}^{-1} = k/l \tag{14}$$

where k is a constant reflecting the vibrational characteristics of the chain. With chain length expressed in chain units, results for lengthy uniform oligo(oxyethylene)s[68] lead to an approximate value of $k = 380$. Other things being equal, an extended E_{30} chain should have a LAM-1 frequency of 12–13 cm^{-1}, while a once-folded E_{30} chain should have a LAM-1 frequency twice as large.

Low-frequency Raman spectra of the solid copolymers are shown in Figure 9. The quality of the spectra obtained for the copolymers made it impossible to define broad peaks of low intensity, but the LAM-1 bands could be picked out, if necessary, by repeatedly recording a particular spectrum so as to isolate the peak from the noise. The LAM-1 frequencies obtained (listed in Table 3) decreased significantly with overall chain length along the series of copolymers $E_{30}B_3$ to $E_{29}B_{20}$. The effect is illustrated in Figure 10a, where values of ν_1, normalized to E_{30} by multiplication by (n/30), are plotted against B-block length. The anomalous result for copolymer $E_{31}B_{30}$ is apparent.

The same frequencies are plotted against reciprocal overall chain length ($m + n$ chain units) in Figure 10b. Within the experimental scatter, the results for copolymers $E_{30}B_3$ to $E_{29}B_{20}$ fit to a straight line which passes through the origin. The equation of the line drawn in Figure 10b, which is a least squares fit to the results, is

$$\nu_1/\mathrm{cm}^{-1} = 320/(m + n) \tag{15}$$

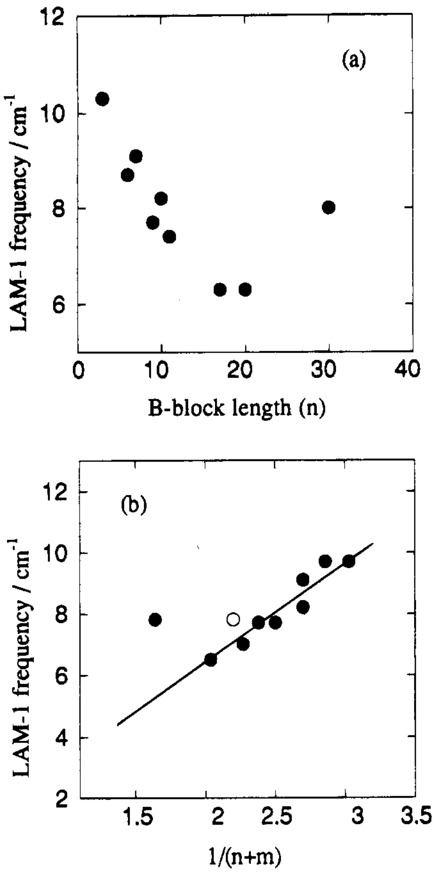

Figure 10. LAM-1 frequencies (from Raman spectroscopy) of crystalline E_mB_n block copolymers (●) $E_{32}B_3$ to $E_{31}B_{30}$. (a) Frequency corrected to constant E-block length (E_{30}) *versus* B-block length (n). (b) Frequency *versus* reciprocal chain length [100/($m + n$)], or for copolymer $E_{31}B_{30}$ (○) *versus* 100/($m + n$/2).

This equation is similar to that (eq 14) established for E_m chains and is consistent with extended copolymer chains (composite chains) having overall vibrational characteristics similar to those of uniform oxyethylene chains of comparable length. In this respect, the Raman data across the range of chain lengths up to $E_{29}B_{20}$ are consistent with either type i or intermediate lamellae, the latter dominated by chains with their E blocks in extended chain conformation. When plotted against reciprocal ($m + n$), the data point for copolymer $E_{31}B_{30}$ lies well off the line of fit for the other copolymers (see Figure 10b) but it comes into approximate coincidence when plotted against ($m + n$/2), as would be expected if its E block was once folded, as in type ii lamellae. It is seen that both SAXS and Raman results can be explained by the same simple models.

3.3.3. Melting Behavior and Degree of Crystallinity from Conventional DSC.

Seven copolymer samples were examined by conventional DSC, together with a sample of methylated PEG1500 (E_{34}): see Table 4. Examples of DSC curves are shown in Figure 11. Curves obtained for stored copolymers with B blocks longer than B_{10} contained secondary peaks at low temperatures. These peaks, which always comprised less than 20% of the total heat of fusion, gave evidence of limited fractionation. DSC curves of self-seeded samples contained single wide peaks: e.g. a spread of ca. 20 K when heated at 10 K min^{-1}.

Table 4. Thermal and WAXS Analysis of Crystalline E_mB_n Block Copolymers

copolymer	T_{pk}/°C	melting range/°C	$\Delta_{fus}H$/ J g^{-1}	w_E	$\Delta_{fus}H_E$/ J g^{-1}	$X_{H,E}$	$X_{W,E}$
$E_{32}B_3$	44	31–47	135	0.87	156	0.78	
$E_{30}B_7$	39	22–41	111	0.72	153	0.78	0.8
$E_{32}B_{10}$	43	30–44	108	0.66	163	0.81	0.8
$E_{26}B_{13}$	35	18–38	78	0.55	143	0.75	0.8
$E_{27}B_{17}$	35	20–39	59	0.49	118	0.62	0.6
$E_{29}B_{20}$	37	20–41	64	0.47	136	0.70	0.7
$E_{31}B_{30}$	35	19–38	56	0.39	147	0.75	0.7

[a] T_m = melting temperature defined by maximum and corrected for thermal lag: uncertainty, ±1 °C. $\Delta_{fus}H$ = enthalpy of fusion per gram of copolymer: uncertainty, ±5 J g^{-1}. $\Delta_{fus}H_E$ = enthalpy of fusion per gram of oxyethylene in the copolymer: uncertainty, ±10 J g^{-1}. $X_{H,E}$ = fractional crystallinity of E block from DSC: uncertainty, ±0.05. $X_{W,E}$ = approximate fractional crystallinity of E block from WAXS: uncertainty, ±0.1.

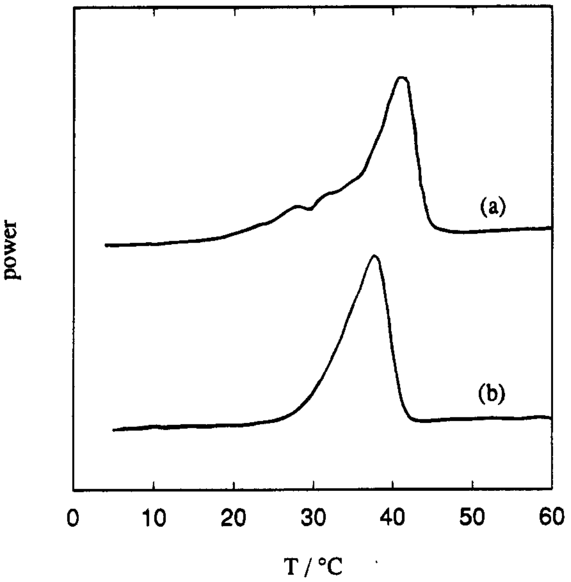

Figure 11. DSC curves (heating rate 10 K min^{-1}) obtained for copolymer $E_{26}B_{13}$: (a) as stored; (b) crystallized by cooling from 60 to 0 °C at −10 K min^{-1}, heated to 40 °C for 1 h, and finally quenched to 0 °C. The temperature scales are uncorrected for thermal lag. The power scales and zeros are arbitrary.

Values of melting temperatures (defined by the maxima in the DSC curves and corrected for thermal lag) and enthalpies of fusion are given in Table 4. The values listed are averages over several determinations. For any one sample, values of $\Delta_{fus}H$ varied by approximately ±5 J g^{-1}, and values of T_m by ±1.5 °C.

Enthalpies of fusion per gram of poly(oxyethylene) in the copolymer were calculated from the measured enthalpy of fusion ($\Delta_{fus}H$) and the weight fraction of oxyethylene in the copolymer (w_E) from

$$\Delta_{fus}H_E = \Delta_{fus}H/w_E \qquad (16)$$

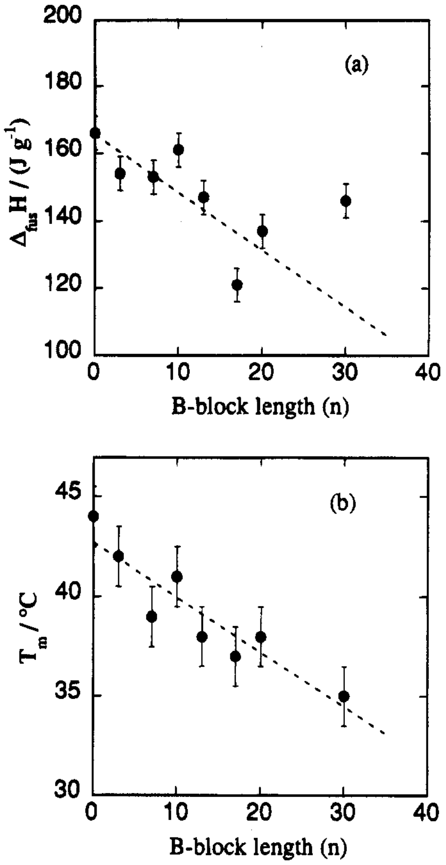

Figure 12. Differential scanning calorimetry of E_mB_n block copolymers. (a) Enthalpy of fusion and (b) melting temperature (temperature at endotherm peak maximum corrected for thermal lag) versus B-block length (n). The data are corrected to constant E-block length (E_{30}). The straight lines drawn through the points (by least squares) have no theoretical implications, but are intended to lead the eye toward regularity of behavior in scattered data.

Values of $\Delta_{fus}H_E$ are listed in Table 4. The melting temperatures and enthalpies of fusion of methyl-terminated poly(oxyethylene)s $M_n \approx 1000$ and 2000 g mol^{-1} (E_{23} and E_{45}) are known[69] and provide a guide to the effect of E-chain length on thermodynamic quantities. Similar values for the chain length dependence of T_m and $\Delta_{fus}H_E$ come from much larger data sets for hydroxy-ended poly(oxyethylene)s.[44,70–72] Accordingly, small corrections were made to normalize all results to the same effective E-block length (E_{30}). Corrected values are plotted against B-block length (n) in Figure 12. As can be seen, values of $\Delta_{fus}H_E$ fall with an increase in B-block length to B_{20}. This trend is emphasized in Figure 12a by the dashed line, which was calculated by least squares for the data points at and below B_{20}. The value for the copolymer with the B_{30} block is significantly off line, indicating a higher crystallinity of the E block for that sample. A similar construction for the melting temperatures is shown in Figure 12b. In that case, all the data points fit to a single straight line. This difference in the two thermodynamic quantities reflects the well-known compensation between the enthalpy and entropy of fusion in T_m, i.e.

$$T_m = \Delta_{fus}H/\Delta_{fus}S \qquad (17)$$

A low value of $\Delta_{fus}H$ means a shorter crystal stem, and so more distinguishable choices of the stem from the chain, i.e. a more disordered crystal, hence a lower $\Delta_{fus}S$.

Values of the thermodynamic enthalpy of fusion of poly(oxyethylene), i.e. the enthalpy of fusion of an infinitely thick crystal free from chain ends, have been reported by a number of laboratories.[38,39,70,71] The results vary significantly, e.g. 197 and 218 J g^{-1} at 70 °C for studies based on extrapolation of data for low-molar-mass poly(oxyethylene)s.[70,71] This difference reflects not only differing data sets for ostensibly the same compounds but also the use of different models to treat data for partly crystalline materials. A purely thermodynamic method which avoids model-led extrapolation gave[73] $\Delta_{fus}H° = 209$ J g^{-1} at 70 °C, while one based on uniform oligomers of defined crystallinity gave[38] 208 J g^{-1} at 70 °C. The temperature dependence of $\Delta_{fus}H°$ is known[38,39] so enabling calculation of values at temperatures in the melting range of the present copolymers: i.e. 195–199 J g^{-1} in the temperature range at 35–44 °C. Making use of the most recent information,[38] fractional crystallinities of the E blocks ($X_{H,E}$, see Table 4) were calculated from corrected enthalpies of fusion as

$$X_H = \Delta_{fus}H_E/\Delta_{fus}H_E° \qquad (18)$$

Significant contributions to $\Delta_{fus}H$ come from the exothermic enthalpy of disappearance of lamellar end surface, and from the endothermic enthalpy of mixing of E and B segments in the melt. Consequently, identification of the enthalpy ratio with the fractional crystallinity of the E blocks (eq 18) yields only apparent values. With regard to the segmental mixing, segregation of blocks in the melt should reduce the positive contribution to $\Delta_{fus}H$ from this source. In the present case the effect should not be large.

The recorded fall in $\Delta_{fus}H_E$ over the B-block range B_3 to B_{20} is consistent with extended copolymer chains in lamellae subject to increased disorder resulting from the difficulty of packing the longer B blocks, i.e. consistent with lamellae of type i. The effect embraces the onset of overt fractionation, which (presumably) originates in the distribution of composition in the copolymers, i.e. in distributions of both E- and B-block lengths.

3.3.4. Melting Behavior and Degree of Crystallinity from WAXS/SAXS/DSC. Approximate fractional crystallinities at 5 °C obtained from WAXS and adjusted to take account of oxyethylene content (denoted $X_{W,E}$) are listed in Table 4 . The precision of these results is low, and they can be quoted only to one place of decimals. Nevertheless, comparison with values of fractional crystallinity from conventional DSC ($X_{H,E}$) shows broad agreement. In particular, the two sets of data consistently show a low crystallinity for sample $E_{27}B_{17}$.

The approximate degree of crystallinity from WAXS (X_W) and the relative invariant from SAXS (Q') are plotted against experiment time for samples $E_{30}B_7$ and $E_{27}B_{17}$ (see Figure 13). In each case the thermal cycle was nominally 10 K min^{-1} from 5 to 50 °C, hold for 1 minute at 50 °C, cool at 10 K min^{-1} from 50 to 5 °C, and hold for 10 min. The time frames, each of 6 s, meant that one frame corresponded to 1 deg. For both copolymers, the integrated WAXS intensity fell continuously above frame 20 as the material started to melt, with corresponding maxima in their invariants.

If a simple two-phase model applies, i.e. if each lamella spacing spans a dense crystalline layer and a less-dense noncrystalline layer (liquid-crystalline layer), then the maxima in Q' may be explained. For such a system, with all material included in the lamellar stacks, the invariant is given by the expression

$$Q' = \phi_c(1 - \phi_c)\langle\eta^2\rangle \qquad (19)$$

which is linear in the electron density difference $\langle\eta^2\rangle$ and quadratic in the volume fraction of crystalline polymer, ϕ_c. The $\langle\eta^2\rangle$ term has a small linear temperature dependence originating in the different thermal expansivities of the crystalline and amorphous phases. However the increase in Q' with temperature originating from this term is usually insignificant compared with the effect of the quadratic term, which has a maximum at $\phi_c = 0.5$. On the basis of WAXS and DSC results, copolymer $E_{30}B_7$ (see Figure 13a) was initially 60% crystalline by volume (equivalent to a fractional crystallinity based on E content alone of $X_{W,E} \approx 0.8$; see Table 4). As the material gradually melted, Q' passed through a maximum as the $\phi_c = 0.5$ condition was reached some 10 deg below the melting point, before falling away prior to complete melting. By contrast, copolymer $E_{27}B_{17}$ was only 49 wt % E and therefore should have been below $\phi_c = 0.5$ throughout the heating and cooling process. The weak maximum in its invariant (see Figure 13b) may be attributable to a decrease in ϕ_c due to melting counteracted by an increase in $\langle\eta^2\rangle$ due to heating, but the contribution of SAXS from liquid-crystalline B blocks (consistent with the interpretation of the Raman and SAXS results given above) must also be borne in mind, as well as the possibility that the experiment was complicated by fractionation.

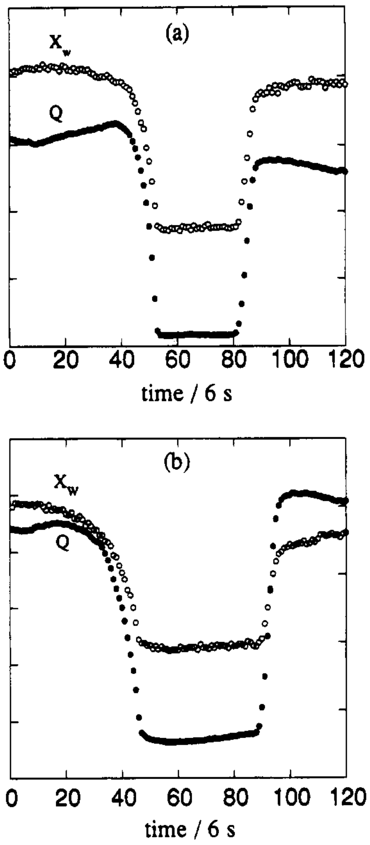

Figure 13. Time dependence of (●) the SAXS invariant Q' and (○) the integrated WAXS intensity X_W during melting and recrystallization of copolymers (a) $E_{30}B_7$ and (b) $E_{27}B_{17}$. The two quantities were calculated as described in the text.

3.3.5. Correlation of the X-ray and DSC Measurements. The DSC curve is the apparent heat capacity versus temperature. In order to check the correlation of the SAXS patterns and the DSC curve, the differentials of the invariant and the integrated WAXS intensities with respect to temperature (i.e. dQ'/dT and dX_W/dT) were calculated. These quantities are plotted together with the simultaneous DSC curve in Figure 14, the data for copolymer $E_{26}B_{13}$ being chosen as its first melting showed relatively complex behavior in the SAXS/WAXS/DSC experiment. As discussed in section 3.3.3, copolymer $E_{26}B_{13}$ exhibits multiple melting behavior in conventional DSC. This behavior is seen in all the data plotted in Figure 14, the changes in the heat capacity on heating the sample, seen in the DSC curve, being reproduced in the dQ'/dT and dX_W/dT

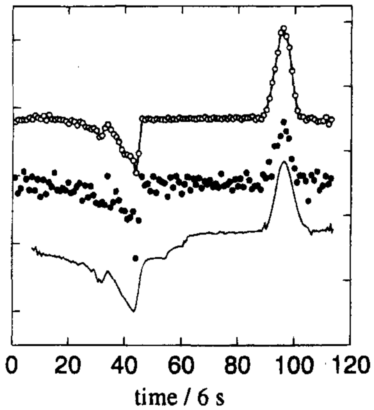

Figure 14. Correlation of DSC and scattering data in the SAXS/WAXS/DSC technique. The data are for copolymer $E_{26}B_{13}$. The temperature differentials of the SAXS invariant dQ'/dT (○) and the fractional crystallinity from WAXS dX_W/dT (●) are plotted with the DSC curve (—). The shoulder on the DSC curve during melting can be observed in both the SAXS and WAXS data.

curves. The peak-to-peak correlation is excellent, due to the timing markers afforded by the simultaneous experiment. Equally, the maxima in the crystallization curves obtained on cooling the copolymer map exactly onto one another within the time resolution of the X-ray experiments.

As seen in Figure 14, the SAXS data are intrinsically less noisy than the WAXS data. There are two reasons for this: the count rate of the WAXS detector is 10^3 times less than that of the SAXS detector and, secondly, the whole of the SAXS pattern is used in calculating Q' whereas only a small fraction of the WAXS pattern is integrated to obtain X_W.

3.4. Concluding Remarks. The experiments concern a series of copolymers with constant E-block length (30 ± 4 E units) and various B-block lengths (3–30 B units), all with narrow chain length distributions ($M_w/M_n < 1.08$). Molar masses were in the range 1600–3500 g mol^{-1}, with number average lengths in the range 100–180 chain atoms. Because of the constant E-block length and the short overall chain length, the copolymers were best suited to an investigation of solid-state properties. Nevertheless, SAXS from the copolymer melts provided new information on short copolymer chains near to their order–disorder transition.

3.4.1. Liquid Copolymers. The SAXS patterns found for the liquid copolymers were consistent with disordered systems, with the melts of the longer copolymers close enough to the ODT to show substantial contributions to SAXS from composition fluctuations. Within experimental error, the characteristic periodicity of the fluctuations scaled as the half power of statistical chain length, in good agreement with theory[16] for unstretched chains. We note the assumptions made in calculating the parameters used to interpret these data, which were made necessary through lack of relevant information. We hope to remedy this situation in the near future.

3.4.2. Solid Copolymers. Copolymers in the range $E_{32}B_3$ to $E_{29}B_{20}$ formed a set of samples which displayed regular behavior in all measured properties of their solid states, whereas the properties of copolymer $E_{31}B_{30}$ differed.

The evidence is that copolymers $E_{32}B_3$ to $E_{29}B_{20}$ formed lamellae in which the whole chain was in extended conformation. These lamellae are denoted type i. The evidence from SAXS and Raman spectroscopy is very strong. The structure has extended E blocks crystallized in their usual helical conformation and B blocks in trans-planar (or similar) conformation in a liquid-crystalline array. Because of the large area of cross-section of the B blocks, type i lamellae cannot readily accommodate uniform arrays of chains, and the systems became increasingly disordered as the B-block length was increased (evidence from DSC). For copolymers with average B-block length $n < 13$, the excess volume of the B blocks caused an increase in lamellar thickness with B-block length. In the range $n = 13$–20, the relative lamellar spacing (d_c/l_c) decreased from its maximum value. This effect coincided with the onset of fractionation, as detected by DSC and SAXS/WAXS/DSC, which served as a second mechanism for alleviation of the packing problem. This effect may be connected with the onset of E-block folding, but direct evidence that this was the case was not obtained.

In the case of copolymer $E_{31}B_{30}$, a partly-folded chain conformation predominated, i.e. a once-folded E block combined with an extended B block. Lamellae of this type are denoted type ii. Again the evidence from SAXS and Raman spectroscopy is strong, and a relatively high enthalpy of fusion (compared to copolymer $E_{29}B_{20}$) provides additional evidence of an abrupt change in crystal morphology between copolymers $E_{29}B_{20}$ and $E_{31}B_{30}$.

Because, other things being equal, the stability of folded-chain crystals is lower than that of extended-chain crystals, chain folding of the crystalline blocks under given crystallization conditions must be driven by a lowering of Gibbs energy of the blocks in the noncrystalline layers, and the general prediction is that this will occur provided that the noncrystallizable blocks exceed a critical length. The importance of the length of the B block is particularly clear in the results obtained for the $E_{30}B_n$ system.

Previous experimental work on diblock copolymers with one poly(oxyethylene) block has largely concerned samples with relatively lengthy blocks, typically each exceeding 100 chain units. Examples are poly(oxyethylene)/poly(styrene)[30,31,74,75] and poly(oxyethylene)/poly(butadiene)[31,75] block copolymers. For example, the average number of chain folds (estimated from SAXS measurements) in crystalline E_{230} blocks ($M_n \approx 10\,000$ g mol^{-1}) of the above copolymers were found[75] to be 10 or more. In contrast, Galin and Mathis,[34] who studied the structures of semicrystalline poly(dimethylsiloxane)/poly(oxyethylene)/poly(dimethylsiloxane) triblock copolymers with lengthy E blocks and end blocks up to DMS_{60}, found relatively low extents of chain folding, comparable to that in crystalline poly(oxyethylene) of a similar chain length.

Structures of a number of E_mP_n and $P_mE_nP_m$ copolymers (P = oxypropylene), and E_mC_n and $C_nE_mC_n$ copolymers (C_n = alkyl) have been determined.[45–48,76–78] These copolymers had E blocks less than E_{80} and relatively short end blocks. For crystallization temperatures in the range 20–40 °C, once-folded conformations were clearly confirmed (by combined SAXS and Raman spectroscopy), but only for those samples with overall chain lengths greater than 150–160 chain atoms. This critical chain length is similar to that (ca. 170 chain atoms) determined for incipient chain folding in homo- and block-oligomers (see section 1.2). It seems that the kinetic factors which determine chain folding in the crystallization of homopolymer chains apply equally to these E/P and E/C block copolymers, i.e. initially the whole chain folds.

The chain folding observed for copolymer $E_{31}B_{30}$ differs in combining a folded E block with an extended B block. To our knowledge this type ii chain folding has not been reported before. As discussed above, we attribute the chain folding to the relatively large area of cross-section of the extended B block compared with the extended E block and, in contrast to the other systems described above, ascribe it to an equilibrium (thermodynamic) effect. This corresponds in principle to existing theoretical treatments of block copolymer crystallization,[41-43] but the details differ, since the noncrystalline B blocks are extended in the present case.

Acknowledgment. We are pleased to acknowledge interesting discussions with Prof. F. S. Bates and Dr. I. W. Hamley. Mr. K. Nixon, Mr. M. Hart, and Mr. P. Kobryn helped with the measurements. Financial support came from the Government of the Republic of China, the Institute for the Promotion of Teaching Science and Technology of Thailand, the Royal Society, the British Council, and the Engineering Physical Sciences Research Council.

References and Notes

(1) *Block Copolymers*; Aggerwal, S. L., Ed.; Plenum: New York, 1970.
(2) *Developments in Block Copolymers-1*; Goodman, I., Ed.; Applied Science: New York, 1982.
(3) *Processing, Structure and Properties of Block Copolymers*; Folkes, M. J., Ed.; Elsevier: New York, 1985.
(4) *Thermoplastic Elastomers*; Legge, N. R., Holden, G., Schroeder, H. E., Eds.; Hanser: New York, 1987.
(5) Brown, R. A.; Masters, A. J.; Price, C.; Yuan, X.-F. In *Comprehensive Polymer Science*; Booth, C., Price, C., Eds.; Pergamon: Oxford, U.K., 1989, Chapter 6.
(6) Elwell, M. J. E.; Ryan, A. J.; Grünbauer, H. J. M.; Van Lieshout, H. C.; Thoen, J. A. *Prog. Rubber Plas. Technol.* **1993**, *9*, 120.
(7) Lunsted, L. G. *J. Am. Oil Chem.* **1951**, *28*, 294.
(8) Holden, G.; Bishop, E. T.; Legge, N. R. *Proceedings of the International Rubber Conference*; MacLaren: London, 1968; p 287.
(9) *B-Series Polyglycols. Butylene Oxide/Ethylene Oxide Block Copolymers*; Technical literature; Dow Chemical Co.: Freeport, TX, 1994.
(10) Tanodekaew, S.; Deng, N.-J.; Smith, S.; Yang, Y.-W.; Attwood, D.; Booth, C. *J. Phys. Chem.* **1993**, *97*, 11847.
(11) Heatley, F.; Yu, G.-E.; Sun, W.-B.; Pywell, E. J.; Mobbs, R. H.; Booth, C. *Eur. Polym. J.* **1990**, *26*, 583.
(12) Moleau, G. E. In ref 1, p 102.
(13) Bates, F. S.; Fredrickson, G. H. *Annu. Rev. Phys. Chem.* **1990**, *42*, 525.
(14) Helfand, E.; Wasserman, Z. R. In ref 2, Chapter 4.
(15) Liebler, L. *Macromolecules* **1980**, *13*, 1602.
(16) Fredrickson, G. H.; Helfand, E. *J. Chem. Phys.* **1987**, *87*, 697.
(17) Almdal, K.; Rosedale, J. H.; Bates, F. S.; Wignall, G. D.; Fredrickson, G. H. *Phys. Rev. Lett.* **1990**, *65*, 1112.
(18) Banaszak, M.; Whitmore, M. D. *Macromolecules* **1992**, *25*, 249.
(19) Shull, K. R. *Macromolecules* **1992**, *25*, 2122.
(20) Vavasour, J. D.; Whitmore, M. D. *Macromolecules* **1992**, *25*, 5477.
(21) Almdal, K.; Koppi, K. A.; Bates, F. S.; Mortensen, K. *Macromolecules* **1992**, *25*, 1743.
(22) Hamley, I. W.; Bates, F. S. *J. Chem. Phys.* **1994**, *100*, 6831.
(23) Förster, S.; Khandpur, A. K.; Zhao, J.; Bates, F. S.; Hamley, I. W.; Ryan, A. J.; Bras, W. *Macromolecules* **1994**, *27*, 6922.
(24) Helfand, E.; Sapse, A. M. *J. Chem. Phys.* **1975**, *62*, 1327.
(25) Vavasour, J. D.; Whitmore, M. D. *Macromolecules* **1993**, *26*, 7070.
(26) Simon, F. T.; Rutherford, J. M. *J. Appl. Phys.* **1964**, *35*, 82.
(27) *B-Series Polyglycols. Polybutylene Glycols*; Technical Literature; Dow Chemical Co.: Freeport, TX, 1994.
(28) Beech, D. R.; Booth, C. *J. Polym. Sci., Polym. Phys. Ed.* **1969**, *7*, 575.
(29) Booth, C.; Orme, R. *Polymer* **1970**, *11*, 626.
(30) Skoulios, A.; Finaz, G.; Parrod, J. *C. R. Hebd. Seances Acad. Sci.* **1960**, *251*, 739.
(31) Gevais, M.; Gallot, B. *Makromol. Chem.* **1973**, *171*, 157.
(32) Cohen, R. E.; Chang, P. L.; Douzinas, K.; Kofinas, P.; Berney, C. V. *Macromolecules* **1990**, *23*, 324.
(33) Nojima, S.; Kato, K.; Yamamoto, S.; Ashida, T. *Macromolecules* **1992**, *25*, 2237.
(34) Galin, M.; Mathis, A. *Macromolecules* **1981**, *14*, 677.
(35) Rangarajan, P.; Register, R. A.; Fetters, L. J. *Macromolecules* **1993**, *26*, 4640.
(36) Ryan, A. J.; Hamley, I. W.; Bras, W.; Bates, F. S. *Macromolecules* **1995**, *28*, 3860.
(37) Yeates, S. G.; Booth, C. *Eur. Polym. J.* **1985**, *21*, 217.
(38) Campbell, C.; Viras, K.; Richardson, M. J.; Masters, A. J.; Booth, C. *Makromol. Chem.* **1993**, *194*, 799.
(39) Domszy, R. C.; Mobbs, R. H.; Leung, Y. K.; Heatley, F.; Booth, C. *Polymer* **1979**, *20*, 1204; **1980**, *21*, 588.
(40) Perret, R.; Skoulios, A. *Makromol. Chem.* **1972**, *162*, 163.
(41) DiMarzio, E. A.; Guttman, C. M.; Hoffmann, J. D. *Macromolecules* **1980**, *13*, 1194.
(42) Whitmore, M. D.; Noolandi, J. *Macromolecules* **1988**, *21*, 1482.
(43) Viglis, T.; Halperin, A. *Macromolecules* **1991**, *24*, 2090.
(44) Nace, V. M.; Whitmarsh, R. H.; Edens, M. W. *J. Am. Oil Chem. Soc.* **1994**, *71*, 777.
(45) Ashman, P. C.; Booth, C. *Polymer* **1975**, *16*, 889.
(46) Booth, C.; Pickles, C. J. *J. Polym. Sci., Polym. Phys. Ed.* **1973**, *11*, 249.
(47) Ashman, P. C.; Booth, C.; Cooper, D. R.; Price, C. *Polymer* **1975**, *16*, 897.
(48) Viras, F.; Luo, Y.-Z.; Viras, K.; Mobbs, R. H.; King, T. A.; Booth, C. *Makromol. Chem.* **1988**, *189*, 459.
(49) Simek, L.; Petrik, S.; Hadobas, F.; Bohdanecky, M. *Eur. Polym. J.* **1990**, *26*, 371.
(50) Heatley, F.; Luo, Y.-Z.; Ding, J.-F.; Mobbs, R. H.; Booth, C. *Macromolecules* **1988**, *21*, 2713.
(51) Yu, G.-E.; Masters, A. J.; Heatley, F.; Booth, C.; Blease, T. G. *Macromol. Chem. Phys.* **1994**, *195*, 1517.
(52) Ungar, G.; Stejny, J.; Keller, A.; Bidd, I.; Whiting, M. C. *Science* **1985**, *229*, 386.
(53) Lee, K. S.; Wegner, G. *Makromol. Chem. Rapid Commun.* **1985**, *6*, 203.
(54) Yeates, S. G.; Booth, C. *Makromol. Chem.* **1985**, *186*, 2663.
(55) Bedells, A. D.; Arafeh, R. M.; Yang, Z.; Attwood, D.; Heatley, F.; Padget, J. C.; Price, C.; Booth, C. *J. Chem. Soc., Faraday Trans.* **1993**, *89*, 1235.
(56) Bras, W.; Derbyshire, G. E.; Ryan, A. J.; Mant, G. R.; Felton, A.; Lewis, R. A.; Hall, C. J.; Greaves, G. N. *Nucl. Instrum. Methods Phys. Res.* **1993**, *A326*, 587.
(57) Ryan, A. J. *J. Thermal Anal.* **1993**, *40*, 887.
(58) Bras, W.; Derbyshire, G. E.; Clarke, S.; Devine, A.; Komanschek, B. U.; Cooke, J.; Ryan, A. J. *J. Appl. Crystallogr.* **1995**.
(59) Ryan, A. J.; Bras, W.; Mant, G. R.; Derbyshire, G. E. *Polymer* **1994**, *35*, 4537.
(60) Takahashi, Y.; Tadokoro, H. *Macromolecules* **1973**, *6*, 881.
(61) Viras, K.; King, T. A.; Booth, C. *J. Polym. Sci., Polym. Phys. Ed.* **1985**, *23*, 471.
(62) Matsuura, H.; Fukuhara, K. *J. Phys. Chem.* **1987**, *91*, 6139.
(63) Allen, G.; Chai, Z.; Chong, C. L.; Higgins, J. S.; Tripathi, J. *Polymer* **1984**, *25*, 239.
(64) Cooper, D. R.; Booth, C. *Polymer* **1977**, *18*, 164.
(65) Friday, A.; Cooper, D. R.; Booth, C. *Polymer* **1977**, *18*, 171.
(66) Craven, J. R.; Zhang, H.; Booth, C. *J. Chem. Soc., Faraday Trans.* **1991**, *87*, 1183.
(67) Flory, P. J. *Statistical Mechanics of Chain Molecules*, Interscience: New York, 1969; p 165.
(68) Campbell, C.; Viras, K.; Booth, C. *J. Polym. Sci., Polym. Phys. Ed.* **1991**, *29*, 1613.
(69) Marshall, A.; Domszy, R. C.; Teo, H. H.; Mobbs, R. H.; Booth, C. *Eur. Polym. J.* **1981**, *17*, 885.
(70) Buckley, C. P.; Kovacs, A. J. *Prog. Colloid Polym. Sci.* **1975**, *58*, 44.
(71) Romankevich, O. V.; Frenkel, S. Ya. *Polym. Sci. USSR* **1980**, *22*, 2647.
(72) Ashman, P. C.; Booth, C. *Polymer* **1972**, *13*, 459.
(73) Booth, C.; Devoy, C. J.; Gee, G. *Polymer* **1971**, *12*, 327. Devoy, C. J. Ph.D. Thesis, University of Manchester, 1966.
(74) Lotz, B.; Kovacs, A. J.; Bassett, G. A.; Keller, A. *Kolloid. Z.-Z. Polym.* **1966**, *209*, 115.
(75) Gervais, M.; Gallot, B. *Makromol. Chem.* **1977**, *178*, 1577.
(76) Booth, C.; Domszy, R. C.; Leung, Y.-K. *Makromol. Chem.* **1979**, *180*, 2765.
(77) Al Kafaji, K. H.; Booth, C. *Makromol. Chem.* **1981**, *182*, 3671.
(78) Cooper, D. R.; Leung, Y.-K.; Heatley, F.; Booth, C. *Polymer* **1978**, *19*, 309.

MA950210+